CT-Operated Bifunctional Fluorescent Probe Based on a Pretwisted Donor–Donor–Biphenyl

Y. Q. Li,[1,2] J. L. Bricks,[3] U. Resch-Genger,[1,5] M. Spieles,[1] and W. Rettig[4]

Taking into account the structural requirements for TICT-type sensor molecules, a general synthetic route to derive pH and cation-responsive pretwisted donor (D)–donor (D) biphenyls (b) equipped with donor receptors is developed and a first model compound containing a mono aza-15-crown-5 and a DMA receptor is synthesized, see Scheme 1. The spectroscopic properties of this new bifunctional D–D biphenyl are studied in the non-polar and polar solvents cyclohexane, acetonitrile, and methanol. Protonation as well as complexation studies are performed with the representative metal ions Na(I), K(I), Ca(II), Ag(I), Zn(II), Cd(II), Hg(II), and Pb(II) to reveal the potential of this molecule for communication of whether *none*, *only one*, or *both binding sites* are engaged in analyte coordination by spectroscopically distinguishable outputs. The results are compared to those obtained with closely related donor (D)–acceptor (A) substituted biphenyl-type sensor molecules and are discussed within the framework of neutral and ionic D – A biphenyls.

KEY WORDS: Fluorescent probe; biphenyl; TICT; photophysics; bifunctional.

INTRODUCTION

In biology, clinical chemistry, and environmental analysis, sensitive and selective fluorescent reporters are desired that enable the determination of either beneficial or harmful metal ions [1,2]. The ideal fluorescent probe should e.g. communicate analyte recognition either selectively or as a sum parameter with strong changes in energy and intensity of absorption and emission as well as of the fluorescence lifetime under application-relevant conditions in the long wavelength region. Well suited sensor molecules that meet at least some of these criteria are of composite design and combine an auxochrome generating the fluorescence signal—via a saturated or unsaturated spacer—with an analyte-responsive receptor

[3]. The sensing properties of such systems depend on the receptor-controlled (chemical) selectivity and the analyte-mediated signaling (spectroscopic) selectivity as well as sensitivity with the underlying photophysical mechanisms and the nature of the receptor–fluorophore interactions determining whether the fluorescence signal is modified in intensity and lifetime and/or in energy [3–5]. The majority of fluorescent reporters that reveal chelation-induced spectral changes are charge transfer (CT)-operated systems with the electronically coupled receptor and chromophore acting as donor and acceptor moieties [6]. For typically used electron donating binding sites like e.g. nitrogen-containing ligands, cation complexation is accompanied by strong blue shifts in absorption as a response to the coordination-induced reduction of the electron donating character of the receptor. However, such intrinsic sensor molecules display normally at maximum only very small spectral changes in emission due to the release or decoordination of the metal ion upon electronic excitation of the complexed probe [7–11]. This hampers true ratiometric emission sensing [12]. Excited-state ion expulsion or decoordination can

---

[1] Federal Institute for Materials Research and Testing (BAM), Working Group Optical Spectroscopy, Berlin, Germany.
[2] National Nanotechnology Laboratory, Lecce University, Lecce, Italy.
[3] Institute of Organic Chemistry, National Academy of Sciences of the Ukraine, Kiev, Ukraine.
[4] Institut für Chemie, Humboldt Universität zu Berlin, Berlin, Germany.
[5] To whom correspondence should be addressed. E-mail,

be avoided if the receptor is integrated into the acceptor part of the molecule [13–16]. This has been realized e.g. for biphenyl-type molecules equipped with pH- and cation-responsive terpyridine acceptors. Such a probe design concept can be established even for azacrown-type receptors in amide-type molecules [17–20], see exemplary compound **2** in Scheme 1. A further benefit of electron accepting binding sites are analytically favorable, coordination-induced strong red shifts not only in absorption, but especially in emission which can principally provide an enhanced sensitivity compared to blue shifted spectra. This, however, requires a sufficiently strong emission of the acceptor-coordinated probe molecule. This can be, for instance, found for molecules that display an anti-energy gap-type behavior [13–15,21], i.e., red shifted emission spectra and still comparatively strong fluorescence quantum yields that are in some cases even enhanced compared to the parent probe. Other approaches towards ratiometric emission signaling include participation of the acceptor fluorophore in cation coordination by the donor receptor [22,23], a D–D design with analyte-mediated transformation of the donor receptor into an acceptor [24,25], the combination of two CT processes in a more complex D^1–A–D^2 type design [26–29] or analyte-mediated introduction of a CT process [30]. If both donor and acceptor moieties or both donors are chosen to be pH- and/or cation-responsive [31,32], bifunctional CT-operated fluorescent probes result, which can in principle signal two chemical inputs by spectroscopically distinguishable outputs. Chemical inputs can be here either two different concentration regimes of a single analyte or two different analytes. Recent developments of such simple bifunctional D–A probes include e.g. donor-substituted biphenyls incorporating terpyridine and bisthienyl-pyridine acceptor receptors [13–15].

For the systematic study and comparison of these different design concepts of CT-operated mono- and bifunctional fluorescent reporters, biphenyls are an interesting class of molecules. From a photophysical point of view, the conformational control of the CT character of D–A-substituted biphenyls [33–41] is linked to the formation of TICT states [42], which combine CT with a twisting of two aromatic subsystems close to perpendicularity [42]. In this way, nearly full electron transfer can be achieved as well as relatively long fluorescence lifetimes due to the more forbidden character of the emission [41, 42]. As an extension of our studies on D–A biphenyls and D–A biphenyl-type fluorescent sensors for protons and metal ions, we designed a first D^1–D^2 biphenyl sensor molecule equipped with two donor receptors (D^1, D^2) and sterically hindering methyl groups as a model system for bifunctional TICT-type fluorescent probes, see molecule
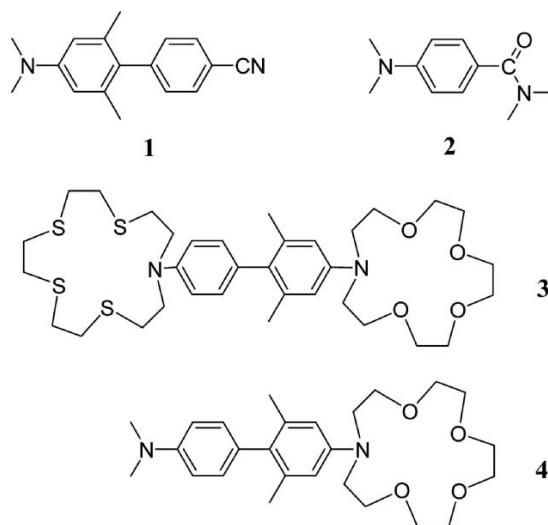
Scheme 1. Chemical structures of selected D–A biphenyl TICT model compounds and newly developed D–D biphenyl sensor molecules.

4 in Scheme 1. D^1–D^2 biphenyls are normally unable to populate TICT states (for first examples of TICT forming D–D molecules, see [43]). However, mono-coordination of such a sterically hindered D^1–D^2 biphenyl that transforms one of the donors into an acceptor is expected to yield a TICT-forming system and accordingly strong red shifts in absorption and especially in emission. Moreover, this transformation should enable strong analyte-mediated changes in fluorescence lifetime. This provides the basis for both ratiometric emission sensing and enhanced cation selectivity via measurement of the additional parameter fluorescence lifetime. Biphenyl-based TICT systems are especially advantageous in this respect because some of these molecules like e.g. compound **1** in Scheme 1 possess a relatively high quantum yield of the TICT emission [13, 14,38,44].

In a first step towards this goal, we synthesized molecule **4** shown in Scheme 1 as prototype of such a pretwisted pH- and cation-responsive D–D biphenyl-crown system, in the simplest version with an integrated azacrown receptor and a dimethylamino donor. Incorporation of donor receptors of varying analyte selectivity eventually enables fine-tuning of the analyte selectivity of this class of fluorescent probes [6,31,45]. As potential candidate, molecule **3** is exemplary shown in Scheme 1. In a first step, the spectroscopic properties of **4** are investigated in the representative solvents cyclohexane, acetonitrile, and methanol. In a second step, coordination-induced effects on absorption and emission spectra, fluorescence quantum yields, and fluorescence lifetimes are studied for protons and the representative non-quenching metal ions

Na(I), K(I), Ca(II), Ag(I), Zn(II), and Cd(II) as well as the potentially quenching metal ions Hg(II) and Pb(II) [4,46].

EXPERIMENTAL

Solvents and Reagents

All the chemicals used for the synthesis of the fluorescent probe **4** were purchased from Merck and Fluka. The metal ion perchlorates obtained from ALFA were of the highest purity commercially available and dried in a vacuum oven before use [47]. All the solvents employed were of spectroscopic grade and obtained from Aldrich. Prior to use, each solvent was checked for fluorescent impurities.

Synthesis

The sterically hindered D^1–D^2 sensor molecule **4** was synthesized from 4-bromo-N,N-dimethylaniline, 4-(neopentyl glycolatoboron)-N,N-dimethylaniline, and 13-(4-bromo-3,5-dimethylphenyl)-1,4,7,10-tetraoxa-13-azacyclopentadecane as depicted in Scheme 2 and described in detail in this section.

4-(Neopentyl glycolatoboron)-N,N-dimethylaniline (**5**). A Schlenk tube was filled with Pd(dppf)Cl$_2$ (60 mg, 7.2×10^{-5} mol, 0.06 eq.), KOAc (0.706 g, 7.2 mmol, 6 eq.) and B$_2$neo$_2$ [bis(neopentyl glycolato)diboron] (0.570 g, 2.52 mmol, 1.05 eq.) and flushed with argon. After addition of DMSO (24 ml, dried over molecular sieves) and 4-bromo-N,N-dimethylaniline (0.48 g, 2.4 mmol), the reaction mixture was heated at 80°C under argon for 10 h and stirred at room temperature overnight. The reaction mixture was diluted with toluene (80 ml) and methylene chloride (40 ml) and the resulting solution washed with

water. The organic layer was dried over MgSO$_4$ and the solvent removed in vacuo. The crude product was dissolved in 10 ml of CH$_2$Cl$_2$ and methanol (5 ml) was added. Evaporation of CH$_2$Cl$_2$ leads to precipitation of the product as a white solid. Yield: 0.320 g. m.p.: 124–130°C. ^{1}H-NMR (300 MHz, CDCl$_3$), δ (ppm): 0.90 (s, 6H, neo-CH$_3$), 2.86 (s, 6H, N(CH$_3$)$_2$), 3.64 (s, 4H, neo-CH$_2$), 6.61–6.58 (d, $J = 8.6$ Hz, 2H, PhH), 7.61–7.59 (d, $J = 8.6$ Hz, 2H, PhH).

N,N,2′,6′-Tetramethyl-4′-(1,4,7,10-tetraoxa-13-azacyclopentadecane-13-yl)-1,1′-bi-phenyl-4-amine (**4**). After degassing of a mixture of 4-(neopentyl glycolatoboron)-N,N-dimethylaniline (**5**) (0.233 g, 1 mmol), 13-(4-bromo-3,5-dimethylphenyl)-1,4,7,10-tetraoxa-13-azacyclopentadecane (**6**) (prepared with 2,4,4,6-tetrabromo-2,5-cyclohexadien-1-one as the brominating reagent as described in [48]; 0.399, 1 mmol), and toluene (20 ml), aqueous NaOH solution (1 M, 10 ml), and the catalyst Pd(PPh$_3$)$_4$ (25 mg, *ca*. 2 mol%) were added and the mixture was stirred under reflux for 20 h under argon. The layers were separated and the aqueous phase was extracted with toluene (4 × 25 ml). The combined organic phases were dried with Na$_2$SO$_4$ and the solvent was evaporated. The remaining solid (0.46 g) was dissolved in hexane, the solution filtered, and the filtrate evaporated. The crude solid (0.43 g) that contains the starting materials and (by)products of the cross-coupling reaction was chromatographed on silica gel using a 1:1 mixture of hexane and ethylacetate as eluent. After evaporation of the solvent, 40 mg of (**5**) was obtained and chromatographed on silica gel with ethylacetate as eluent. Evaporation of the eluent from the last fraction yielded (**4**) that was further purified by recrystallization from hexane. Yield: 0.090 g. ^{1}H-NMR (300 MHz, CDCl$_3$), δ (ppm): 2.14 (s, 6H, CH$_3$Ph), 3.08 (s, 6H, NCH$_3$), 3.73–3.84
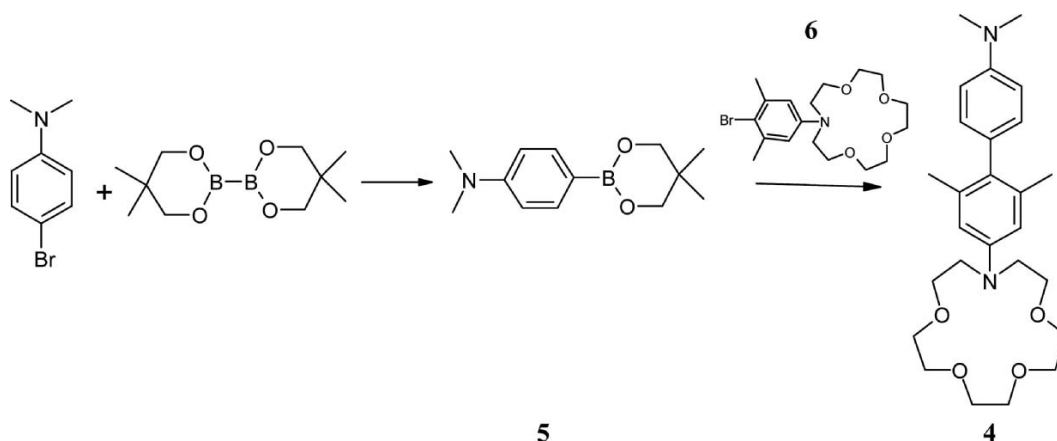
Scheme 2. Synthetic scheme for the preparation of sterically hindered D^1–D^2 biphenyl **4**.

(m, 16H, OCH_2-crown), 3.87–3.92 (t, $J = 6.2$ Hz, 4H, NCH_2-crown), 6.52 (s, 2H, PhH), 6.87–6.90 (d, $J = 8.6$ Hz, 2H, PhH), 7.11–7.14 (d, $J = 8.6$ Hz, 2H, PhH).

Equipment/Procedures

Equipment

The chemical structures of the synthesized compounds were confirmed by elemental analysis,^{1}H NMR, and ^{13}C NMR. Their purity was checked by fluorescence spectroscopy, with excitation wavelength-dependent emission spectra and emission wavelength-dependent excitation spectra typically pointing to the presence of fluorescent impurities. Melting points (uncorrected) were measured with a digital melting point analyzer IA 9100 (Kleinfeld GmbH) and NMR spectra were obtained with a 500 MHz NMR spectrometer Varian Unityplus 500. Elemental analyses that were performed in duplicate were carried out at the Institute of Organic Chemistry, National Academy of Sciences, Ukraine, Kiev, with samples being dried prior to analysis for 5–6 h at 80°C in vacuo following routine procedures.

Steady State Absorption and Fluorescence

The UV/Vis spectra were recorded on a Carl Zeiss Specord M400/M500 and a Bruins Instruments Omega 10 absorption spectrometer. The fluorescence spectra were measured with a Spectronics Instruments 8100 and a Perkin-Elmer LS50B spectrofluorometer. If not otherwise stated, all the fluorescence spectra presented are corrected for the wavelength- and polarization-dependent spectral responsivity of the detection system traceable to the *spectral radiance scale*. This instrument-specific quantity was determined with a calibrated quartz halogen lamp placed inside an integrating sphere and a white standard both from Gigahertz-Optik GmbH in the case of fluorometer 8100 and with spectral fluorescence standards with known corrected emission spectra for fluorometer LS50B following previously described procedures [49]. The emission spectra on a wave number (energy) scale were obtained by multiplying the measured and corrected emission spectra with λ^2 [50]. The absorption and emission maxima given are determined from the respective spectra plotted on an energy scale.

Time—Resolved Fluorescence

Fluorescence decay curves were recorded with the time-correlated single-photon counting technique (TC-SPC) [51] using an Ar-pumped Ti-Sapphire laser as exci-

tation source and a previously described setup [52], as well as with a setup at the Berlin Synchrotron facility BESSY II employing synchrotron radiation as excitation light source in conjunction with an excitation monochromator (Jobin Yvon, II, 10 UV). BESSY II delivers a 1.25 MHz pulse train with characteristic pulse widths of 30–50 ps. The fluorescence decays were detected with a microchannel plate photomultiplier tube (MCP, Hamamatsu R 1564-U-01) cooled to −30°C, coupled to an emission monochromator (Jobin Yvon II, 10 VIR) by means of quartz fiber optics. The signal from a constant fraction discriminator (CFD, Tennelec 454) was used as start pulse for the time-to-amplitude converter (TAC, Tennelec TC864) operating in the reverse mode. The BESSY II synchronization pulse was applied as stop pulse. The MCP pulses were amplified by an amplifier (INA 10386) and coupled into the CFD. A multichannel analyzer (Fast Comtec MCDLAP) was employed for data accumulation. The decays were analyzed by the least squares iterative reconvolution method on the basis of the Marquardt–Levenberg algorithm, which is implemented into the commercial global analysis program [53]. The instrument response function was obtained by detection of Rayleigh scattered light in a scattering solution and had a width of 50–60 ps for the laser setup used and a width of 120 ps in the case of experiments at BESSY II. The quality of the exponential fits was evaluated on the basis of reduced χ^2 values.

Procedures

Fluorescence Quantum Yields

The fluorescence quantum yields (φ_f) were calculated from integrated, blank and spectrally corrected emission spectra (wavelength scale) employing quinine sulfate in 1N H_2SO_4 ($\varphi_f = 0.55 \pm 0.03$) [54] as fluorescence standard. For each compound–solvent pair, the quantum yield was determined twice. The uncertainties of the quantum yield measurement were obtained to $\pm 5\%$ (for $\varphi_f > 0.4$), $\pm 10\%$ (for $0.2 > \varphi_f > 0.02$), $\pm 20\%$ (for $0.02 > \varphi_f > 0.005$), and $\pm 30\%$ (for $0.005 > \varphi_f$), respectively.

Protonation and Complexation Constants

The coordination constants (K_s) for mono-coordination of **4**, i.e., mono-protonation or mono-complexation were determined from the variations of the fluorescence intensity of the emission maximum of either the probe or the mono-coordinated species assuming a 1:1 stoichiometry as described by Valeur [55].

RESULTS

Synthesis of the Pretwisted D^1–D^2 Sensor Molecule 4

The synthesis of **4**, see Scheme 2, has been a challenge to the organic chemist. Although there exists a number of reports of Suzuki reactions of aryl halides that form pretwisted biaryls with *ortho*-substituents, this type of coupling reaction can be difficult requiring special conditions and giving only modest yields [38,56,57].

Biaryls are commonly prepared by the use of a Pd-catalyst such as e.g. $Pd(Ph_3P)_4$ or $(Ph_3P)_2Cl_2$. Our screening studies, however, indicated that 1,1′-bis(diphenylphosphino)ferrocene]palladium(II) chloride ($dppfPdCl_2$) is superior to the conventional Ph_3P-based catalysts and bidentate phosphine-based ligands. Also, the presence of KOAc facilitated the reaction. Application of this improved procedure to the corresponding aryl bromide yielded the pinacolate ester of the desired boronic acid. Nevertheless, deprotection of the resulting boronate to generate the boronic acid was difficult because the pinacol formed a particularly stable boronate ester resistant to hydrolysis under both acidic and basic conditions [58]. However, substitution of the pinacolate for its more readily hydrolizable neopentyl glycolate analogue, i.e., bis(neopentyl glycolato) diboron under conditions otherwise identical to the pinacolate reaction yielded a reactive boronate ester that could be readily employed for the next step of the coupling reaction, see Scheme 2. With this synthetic strategy developed by us and the use of related compounds of **5** and **6** equipped with different macrocyclic receptors, fluorescent reporters like e.g. molecule **3** shown in Scheme 1 or other D^1–D^2 sensor molecules are at reach by straightforward variations of this synthetic procedure.
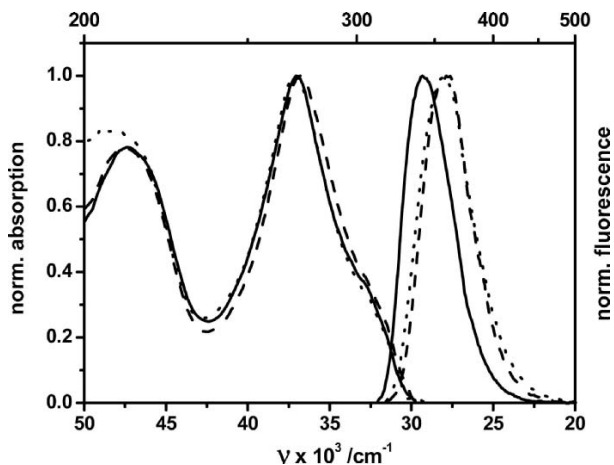

Fig 1. Normalized absorption (*left*) and emission (*right*) spectra of **4** in cyclohexane (solid line), ACN (dashed), and MeOH (short dotted line), ligand concentration 2×10^{-6} M, excitation at 310 nm.

Spectroscopic Properties of 4

The spectroscopic properties of **4** in the representative apolar, polar, and protic solvents cyclohexane (CH), acetonitrile (ACN), and methanol (MeOH) are summarized in Table I and Fig. 1. The absorption spectra of **4** are more or less unaffected by solvent polarity and proticity and the emission spectra display only a little red shift in the strongly polar solvents acetonitrile and methanol. Independent of solvent polarity, the Stokes shift remains small. The fluorescence quantum yield is moderate in all the solvents and decreases only slightly in acetonitrile as compared to apolar cyclohexane. There seems to be a moderate fluorescence quenching effect in methanol as observed for other CT-operated biphenyls [13,38].

Table I. Spectroscopic Properties of **4** in Different Solvents

Solvent	v_{abs}[a] ($\times 10^3 cm^{-1}$)	v_{em}[b] ($\times 10^3 cm^{-1}$)	FWHM[c] ($\times 10^3 cm^{-1}$)	Δv_{St}[d] ($\times 10^3 cm^{-1}$)	ϕ_f[e]	τ_f[f] (ns)	k_f[g] ($\times 10^7 s^{-1}$)	k_{nr}[h] ($\times 10^7 s^{-1}$)
CH	37.0, 32.3 (sh)	29.2	3.5	3.1	0.17	2.4	7	35
ACN	37.0, 32.3 (sh)	27.9	3.5	4.3	0.12	2.6	5	34
MeOH	37.1, 32.3 (sh)	27.9	3.8	4.3	0.09	1.7	5	54

[a]Absorption maxima.
[b]Emission maximum.
[c]Band width, i.e., full width at half height of the maximum.
[d]Stokes shift, i.e., the energetic difference between the longest wavelength absorption band (or shoulder) and the emission maximum.
[e]Fluorescence quantum yield.
[f]Fluorescence lifetime.
[g]Radiative rate constant, $k_f = \phi_f / \tau_f$.
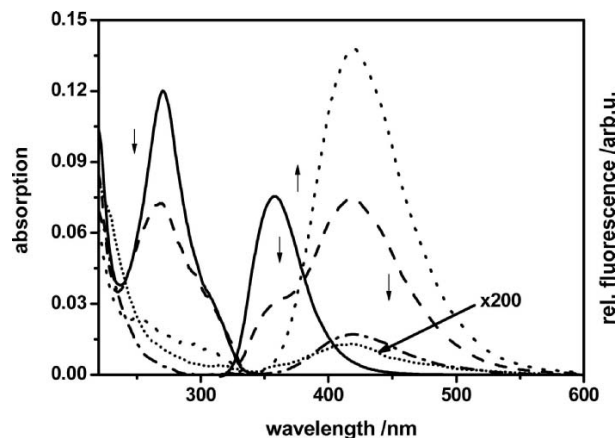[h]Non-radiative rate constant, $k_{nr} = (1 - \phi_f) / \tau_f$.

Fig 2. Absorption (*left*) and emission (*right*) spectra of **4** at selected proton-to-ligand concentration ratios of 0:1 (solid line), 1:1 (dashed), 2:1 (dotted), 3:1 (dash-dotted), and 10:1 (short dotted line). The probe concentration was 4×10^{-6} M, solvent ACN, excitation at 310 nm. The emission of the doubly protonated species cannot be excited at 310 nm due to lack of absorption at this wavelength, see Fig. 3.

Protonation Studies

The protonation-induced effects on the absorption and emission spectra of **4** are displayed in Figs. 2 and 3. Mono-protonation leads to a decrease in the ligand's absorption band and to only very small spectral shifts. No new red shifted absorption band is observed. Simultaneously, the emission band of the sensor molecule at 358 nm disappears, and a new red shifted emission band centered
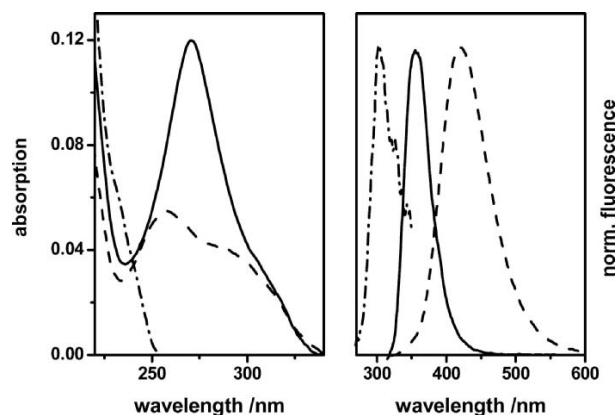

Fig 3. Absorption (*left*) and normalized emission (*right*) spectra of unprotonated (solid line), mono protonated (dashed; 2:1 H$^+$), and doubly protonated (dash-dotted line; 1:1000 H$^+$) **4** in ACN. In the former two cases, the concentration of the probe was 4×10^{-6} M and excitation at 310 nm, whereas in the latter case, the probe concentration was 1.1×10^{-5} M and excitation at 230 nm. The proton-to-ligand concentration ratios are given in the brackets.

at 420 nm occurs. The clear course of mono-protonation of **4** follows from the observation of an isosbestic point at 240 nm. Moreover, an isoemissive point at *ca.* 382 nm is noticed. For complete mono-protonation that is achieved at a 2:1 proton-to-ligand concentration ratio, only the 420 nm band remains, the fluorescence quantum yield of which exceeding that of **4** by a factor of *ca.* 3, see Table II. Upon further addition of acid, the emission band of the mono-protonated species disappears and both the absorption and emission bands are strongly blue shifted as revealed in Figs. 2 and 3. Doubly protonated **4** with its strongly blue-shifted emission band at *ca.* 305 nm is only very weakly emissive.

Complexation Studies

Complexation studies were performed with **4** and the non-quenching metal ions Na(I), K(I), Ag(I), Ca(II), Zn(II), Cd(II) as well as with the potential fluorescence quenchers Pb(II) and Hg(II) in acetonitrile [46]. The results are summarized in Table II and in Fig. 4 that displays the quantum yield-weighted emission spectra of mono-coordinated **II**. Mono-coordination of **4** leads to considerable changes in the intensity of the absorption bands of **4**, whereas their spectral position is barely affected, see Table II and Fig. 5 that displays a representative example of a titration of **4** with a metal ion, here Hg(II). Similar to mono-protonation, also cation mono-coordination of **4** is accompanied by considerable red shifts in emission for Zn(II), Pb(II), and Hg(II) yielding spectrally rather similar species, whereas in the case of Cd(II) and especially Ca(II), smaller shifts occur even at a high excess of the respective metal ion. Mono-coordination of **4** yields isoemissive points at *ca.* 380 nm for Ca(II), Zn(II), and Hg(II), at 393 nm for Pb(II), and at 415 nm for Cd(II), respectively. Chelation-enhanced fluorescence results for non-quenching Ca(II) and Zn(II), and remarkably also for the classical fluorescence quencher Hg(II) [46]. The fluorescence quantum yields of the cation complexes exceed that of the parent probe by factors of 2 and 3, respectively, see Table II. Mono-coordination of **4** to Cd(II) and Pb(II) yields only weakly emissive species. The fluorescence lifetimes of the Zn(II), Hg(II), and Pb(II) complexes of **4** with values of *ca.* 3 ns are slightly increased compared to the parent probe with a lifetime of 2.6 ns, whereas the fluorescence lifetime of the Cd(II) complex is reduced to 1.0 ns. Addition of the metal ions K(I), Na(I), and Ag(I) even at a high excess did not lead to spectroscopically measurable effects.

The potential of **4** to act as bifunctional fluorescent reporter not only for protons but also for metal ions is revealed for Hg(II) in Fig. 5. Upon addition of increasing

Table II. Spectroscopic Properties of Mono- and Double-Protonated **4** and Mono-Coordinated **4** in ACN

Compound	ν_{abs}[a] ($\times 10^3$ cm^{-1})	ν_{em}[b] ($\times 10^3$ cm^{-1})	$\log K_s$[c]	ϕ_f[d]	τ_f[e] (ns)	k_f[f] ($\times 10^7$ s^{-1})	k_{nr}[g] ($\times 10^7$ s^{-1})
4	37.0, 32.3 (sh)	27.9		0.12	2.6	5	34
4⊂H$^+$	32.3	23.8	5.6	0.31	3.5	9	20
H$^+$⊃**4**⊂H$^+$	> 44.4	32.8	n.d.[h]	n.d	0.3	n.d	n.d
4⊂Ca^{2+}	32.3	27.0	5.5	0.19	2.5	8	32
4⊂Cd^{2+}	32.3	25.0	5.0	0.03	1.0	3	97
4⊂Zn^{2+}	32.3	23.8	6.2	0.29	2.9	10	24
4⊂Hg^{2+}	32.3	23.8	5.2	0.19	3.0	6	27
4⊂Pb^{2+}	32.3	23.8	5.3	0.02	2.9	1	34

[a]Absorption maxima.
[b]Emission maximum.
[c]Coordination constant assuming 1:1 stochiometry.
[d]Fluorescence quantum yield.
[e]Fluorescence lifetime.
[f]Radiative rate constant, $k_f = \varphi_f / \tau_f$.
[g]Non-radiative rate constant, $k_{nr} = (1 - \varphi_f)/\tau_f$.
[h]Not determined.

amounts of mercury perchlorate to mono-coordinated **4**, i.e., for metal ion (M)-to-ligand (L) concentration ratios >1:1 (complete mono-coordination), the absorption bands at *ca.* 270 and 310 nm further decrease and disappear at M:L ratios of 8:1. The determination of the blue-shifted absorption band of the newly formed species that is tentatively assigned to doubly coordinated **4**, i.e., Hg^{2+}⊃**4**⊂Hg^{2+} is complicated by the absorption of
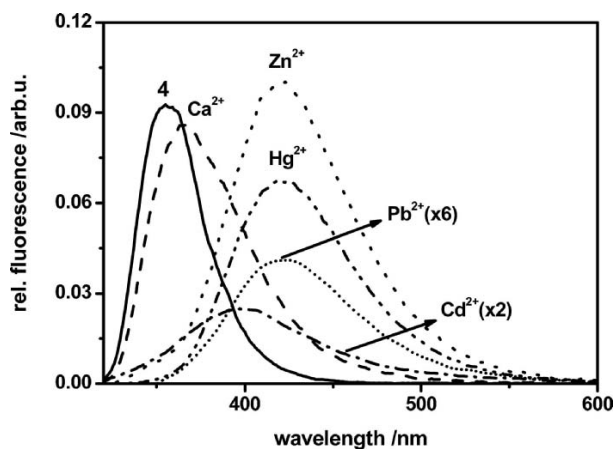

Fig 4. Mono-coordination-induced changes in emission for **4** and selected cations: **4** (solid line), **4**(Ca(II) (dashed; 1:10), **4**(Zn(II) (dotted; 1:10), **4**(Cd(II) (dash-dotted; 1:100), **4**(Hg(II) (dash-dot-dotted; 1:1), and **4**(Pb(II) (short dotted line; 1:1.5). The probe concentration was 4 × 10^{-6} M, solvent ACN, excitation at 310 nm. The metal ion-to-ligand concentration ratios are given in brackets. The emission spectra of the cation complexes are weighted by relative fluorescence quantum yields with the fluorescence quantum yield of the parent probe equaling 1.0.

Hg(ClO$_4$)$_2$ at shorter wavelength. The clear course of formation of Hg^{2+}⊃**4**⊂Hg^{2+} from mono-coordinated **4**, i.e., **4**⊂Hg^{2+} follows from the observation of an isosbestic point at 242 nm. Simultaneously, the emission band of **4**⊂Hg^{2+} at 420 nm decreases. Excitation at shorter wavelengths as used for the excitation of doubly protonated **4**, see Fig. 3, does not lead to a measurable fluorescence. The observed diminution in fluorescence is ascribed to the formation of doubly coordinated **4** which seems to be more or less non-emissive. In the case of Pb(II), where complete mono-coordination of **4** is reached for M:L = 1.5:1, a further increase in Pb(II) concentration up to M:L of 10:1 leads to only very small changes in absorption but to a considerable decrease in fluorescence suggesting contributions from bimolecular quenching. For non-quenching Zn(II), the absorption band of **4**⊂Zn^{2+} and its emission are only barely affected by a further increase in zinc concentration for M:L ratios between 5:1 (complete mono-coordination) and 100:1. Also, in the case of Cd(II) and Ca(II), the lack of spectroscopically measurable changes at high M:L ratios suggests that double coordination cannot be achieved at last at reasonable M:L ratios.

DISCUSSION

We developed a synthetical strategy to derive pretwisted CT-operated D^1–D^2 biphenyl fluorescent reporters like **4** that can be transformed into D–A biphenyls upon protonation or cation coordination of one of the donor receptors. A different strategy towards pretwisted
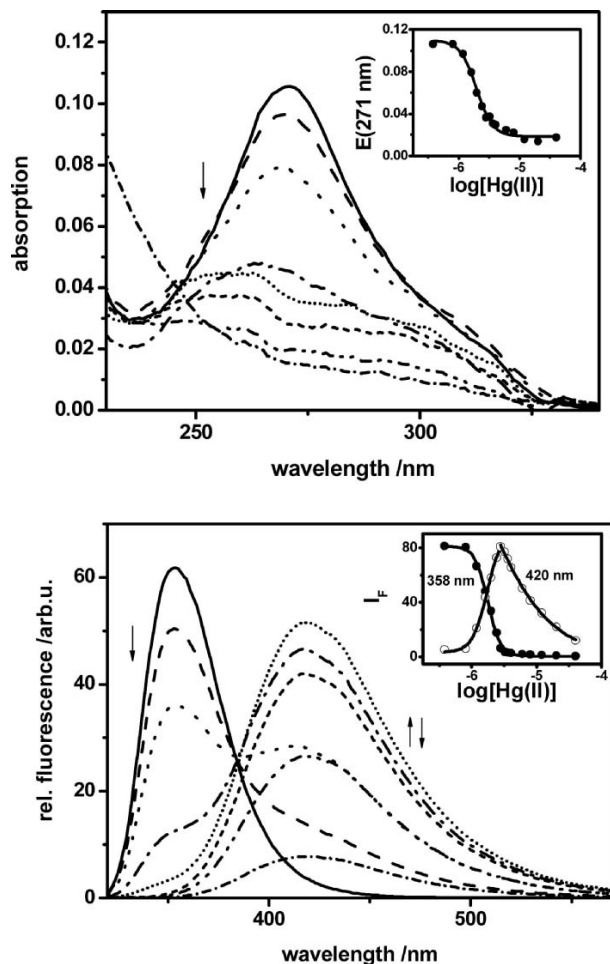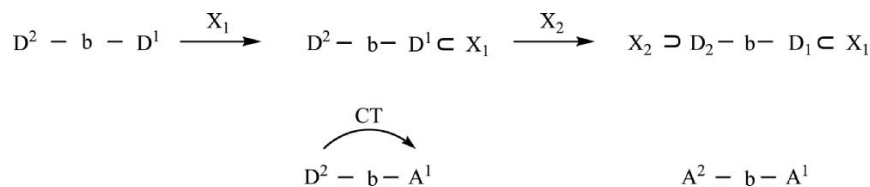
Fig. 5 Successive coordination of both receptors of **4** to Hg(II). Absorption (*left*) and fluorescence (*right*) spectra for Hg(II)-to-ligand concentration ratios of 0:1 (solid line), 0.3:1 (dashed), 0.4:1 (dotted), 0.6:1 (dash-dotted), 0.7:1 (short dotted), 1:1 (short dashed), 2:1 (dash-dot-dotted), and 5:1 (short dash-dotted line) chosen from a titration of **4** with mercury perchlorate. The probe concentration was 4×10^{-6} M, solvent ACN, excitation at 310 nm.

D^1–D^2 biphenyls has been recently presented based on a 4,4′-bis(*N*,*N*-dimethylamino)-biphenyl (TMB, tetramethylbenzidine) subunit equipped with various pH- and cation-responsive *ortho*-substituents thereby providing the basis for analyte-mediated control of the dihedral angle between the two aromatic rings of the biphenyl module [59]. As follows from the steady-state and time-resolved fluorescence measurements described in the previous section, the absorption and fluorescence spectra of **4** are only weakly sensitive to solvent polarity and proticity with the comparatively small values of k_f of (5–7) $\times$ 10^7 s^{-1} found in all solvents used, see Table 1, suggesting a rather forbidden nature of the emissive state even

in apolar cyclohexane. As evidenced by the small solvatochromic red shift of the emission, the low k_f value of **4** does not derive from an intramolecular charge transfer (ICT) state. The k_f value of **4** correlates well with the similarly low k_f value of 3×10^7 s^{-1} obtained for *N*,*N*,*N*′,*N*′-tetramethylbenzidine, TMB [60]. In contrast, typical D–A biphenyls like e.g. 4-*N*,*N*-dimethylamino-4′-cyanobiphenyls reveal k_f values of (40–50) $\times 10^7$ s^{-1} with the exception of pretwisted 4-*N*,*N*-dimethylamino-2,6-dimethyl-4′-cyanobiphenyl **1** [38]. This molecule displays a strongly polarity-sensitive radiative rate constant with values of 30×10^7 and 3×10^7 s^{-1} found in hexane and acetonitrile, respectively, indicative of emission from a forbidden CT state of twisted conformation in highly polar solvents.

As indicated by the mono-coordination induced red shifts in emission, see Table II and Figs. 2–5, the chosen D^1–D^2-design concept—though rarely used [11,24]—is an elegant approach to circumvent release or decoordination of metal ions upon electronic excitation of the complexed probe as revealed by CT-operated fluorescent probes of D–A design with integrated donor receptors [6–10]. Obviously, it can be also used to realize sensor molecules capable of true ratiometric emission signaling. The comparatively small coordination-induced shifts in absorption that allow for excitation at a constant wavelength are in contrast to the substantial shifts in absorption as well as in emission observed for related D–A-substituted biphenyl-type sensor molecules with integrated terpyridine acceptors [13,14]. However, also in the case of the latter molecules, the size of the chelation-induced shifts in emission clearly exceeds those in absorption, and their biphenyl analogues equipped with the weaker electron acceptor bisthienyl-pyridine (2,6-dithien-2-ylpyridine) display only moderate spectral shifts in absorption especially for weak or medium-sized donors [15]. A comparison of protonated **4** and TMB that reveals a larger value of the pK_a (5.6 vs. 4.5–4.7, see Table II) for the former suggests some decoupling of the dialkylamino and azacrown ether groups in **4** with respect to those in TMB due to a twist of these groups induced by the sterically hindering *ortho*-methyl substituents as found in related molecules [61].

The photophysical origin of the protonation- and chelation-induced spectroscopic effects observed for **4** is schematically depicted in Scheme 3. Scheme 3. reveals the mono-coordination-induced transformation of one of the donor receptors into an acceptor substituent and the according switching ON of a CT process which accounts for the red-shifted emission of mono-protonated or mono-complexed **4**. Double coordination turns the remaining donor similarly into an acceptor. The according

$$D^2 - b - D^1 \xrightarrow{\text{X}_1} \quad D^2 - b - D^1 \subset X_1 \xrightarrow{\text{X}_2} \quad X_2 \supset D_2 - b - D_1 \subset X_1$$

$$\xrightarrow{\text{CT}}$$

$$D^2 - b - A^1 \qquad\qquad\qquad A^2 - b - A^1$$

Scheme 3. Spectroscopic effects accompanying mono and double coordination of the D^1–D^2 biphenyl **4**. D^1, D^2: donor receptors, b: biphenyl, X_1, X_2: different chemical inputs, i.e., either different concentrations regimes of the same analyte or two different chemical species, $D^1 \subset X_1$: coordination of receptor D^1 to analyte X_1, A^1, A^2: acceptors.

switching OFF of the mono-coordination-induced CT is responsible for the strongly blue-shifted absorption and emission bands of doubly coordinated **4** compared to mono-coordinated **4** observed for protons and Hg(II), see Figs. 3 and 5, and Table II. The control of the CT character of **4** by its coordination state provides the basis for spectroscopically signaling whether *none*, *only one*, or *both* receptors of this sensor molecule are bound. In the case of a single analyte and different concentration regimes as used here, this corresponds to the inputs *none*, *little*, and *much*.

Time-resolved fluorescence measurements performed with mono-coordinated **4** that provide further information on the electronic nature of the emissive states of these species reveal slightly enhanced k_f values compared to **4** for non-quenching analytes. However, even for mono-protonated **4** and its zinc, mercury, and calcium complex that display the highest fluorescence quantum yields amongst the representative analytes studied, see Table II, k_f reaches at maximum 10×10^7 s^{-1}. In contrast, protonation of sterically non-hindered TMB yields similarly high k_f values as found for 4-N,N'-dimethylamino-4$'$-cyanobiphenyls lacking *ortho*-methyl groups [38,60], the emission of which originating from an allowed ICT state of planar geometry [38]. Similar to **1**, the different behavior of mono-coordinated **4** that present D–A biphenyls, see Scheme 3, can be understood on the basis of the influence of the *ortho*-methyl groups. For these molecules, the introduction of a strong pretwist most likely favors population of a forbidden TICT state. This is revealed, e.g., in the case of **1** by the red shift of its fluorescence band compared to that of its non-hindered analogue and the decrease of the radiative rate constant from *ca.* 40 $\times 10^7$ s^{-1} for 4-N,N'-dimethylamino-4$'$-cyanobiphenyl to 3×10^7 s^{-1} for **1** [38]. The low k_f values and the observed strong red shift in emission found for mono-protonated or -complexed **4** similarly suggest mono-coordination-induced TICT formation with the small radiative rate constants of the parent ligand **4** preventing observation of a coordination-induced decrease of k_f in most cases, see Table II.

From the photophysical point of view, TICT compounds like **1** and mono-coordinated **4** display an interesting behavior. As follows from Table II, the non-radiative rate constants of **4** in acetonitrile slightly decrease upon mono-protonation, as well as upon mono-chelation to zinc and mercury ions despite of the bathochromically shifted emission spectra. The strongest effect, a decrease of k_{nr} by a factor of *ca.* 2 and a bathochromic shift in emission by 4100 cm^{-1} occurs for protons, i.e., for **4**$\subset$H$^+$, see Table II. This diminution of k_{nr} with a simultaneous red shift of the emission is more strongly developed in **1** where k_{nr} decreases by a factor of *ca.* 5, while the fluorescence shifts to the red by more than 8000 cm^{-1} when comparing apolar and highly polar solvents [38]. This red shift in fluorescence accompanied by a reduction of the non-radiative rate constant contradicts the well-established energy gap rule [21] that predicts an increase in k_{nr} with a reduction of the energy gap between the S$_1$ and the ground (S$_0$) state. Such a rare, though analytically favorable anti-energy gap law behavior of TICT compounds that has been observed also for other bifunctional D–A biphenyl-type sensor molecules recently developed by us [13–15] is understandable on the basis of photochemical transitions, i.e., reactions on the excited state hypersurface. TICT formation can be viewed as an adiabatic photoreaction [42], as well as an access to conical intersections of S$_1$ with S$_0$ [62, 63]. Accordingly, the fact that the non-radiative deactivation of the excited state of the non-coordinated fluorescent probe occurs faster than that of the coordination-induced TICT state can be ascribed to different conical intersections occurring for these two excited states. Obviously, the conical intersection depopulating the TICT state of **4**$\subset$H$^+$, **4**$\subset$Zn^{2+}, and **4**$\subset$Hg^{2+} is more difficult to reach than that deactivating the excited state of **4**.

With respect to the analytical potential of **4**, remarkable is the observation of a chelation-enhanced fluorescence not only for protons and non-quenching Ca(II) and Zn(II), but also for the classical fluorescence quencher Hg(II) [46]. The majority of the few fluorescent probes that reveal a coordination-induced switching ON of their emission with mercury ions are electron transfer

(ET) operated [3,4,64,65] rather than CT operated [66, 67]. As has been discussed in the previous sections, the well-separated fluorescence bands of bifunctional **4** and its mono-coordinated analogues provide the basis for true ratiometric emission sensing. This can be exploited for the quantification of protons and metal ions. For the spectral discrimination between different analytes, it is unfavorable that the fluorescence spectra of many of the metal complexes—though red shifted compared to **4**—are rather similar. Only the Ca(II) and the Cd(II) complex can be spectrally distinguished from the Zn(II), Pb(II), and Hg(II) complex of **4** that all display very similar emission spectra. A combination of spectrally resolved and time-resolved emission measurements [68], however, can improve the analyte selectivity of this D^1–D^2-type fluorescent probe with coordination-induced TICT formation. Combined spectral and time-resolved fluorescence measurements for instance should enable discrimination between the cadmium complex of **4** with its reduced fluorescence lifetime of 0.9 ns and $\mathbf{4} \subset Ca^{2+}$ that reveals a fluorescence lifetime of 2.5 ns and a less-pronounced red shift of the emission spectrum, see Table II. Also discrimination between Cd(II) and Zn(II) that is often difficult to establish [68] should be possible, as well as distinction between these cation complexes and the uncomplexed probe. $\mathbf{4} \subset Cd^{2+}$ has a strongly reduced fluorescence lifetime with respect to its zinc analogue and its spectrum is blue shifted, whereas uncomplexed **4** and $\mathbf{4} \subset Zn^{2+}$ that exhibit approximately the same fluorescence lifetime can be readily spectrally discriminated. However, e.g. discrimination between the mercury and lead complex of **4** cannot be achieved on the basis of emission spectra and fluorescence lifetimes.

As representatively revealed in Fig. 5, the consecutive complexation of both receptors of **4** to Hg(II) in combination with the coordination site-specific spectral position of the emission bands provides an extended dynamic range of signaling of a single analyte (up to three decades, see insets in Fig. 5 measured at two different emission wavelengths). This is readily measurable due to the well-separated emission bands and the high fluorescence quantum yield of the ligand and its mono-coordinated complex. The Hg(II) selectivity and usable concentration regime could be for instance fine-tuned upon introduction of a sulfur analogue of the crown incorporated into **4** [31] as illustrated in molecule **3** shown in Scheme 1.

CONCLUSION

A new CT-operated benzidine-related D^1–D^2-type fluorescent probe has been derived that is transformed from a D–D sensor molecule into a D–A system upon mono-coordination and into a A–A system upon double coordination. Sterically hindering *ortho*-methyl groups act as triggers for the introduction of TICT formation in the mono-coordinated species with the corresponding strong analyte-mediated red shift in emission enabling true ratiometric emission sensing of protons and metal ions. Due to the coordination-site control of its CT character, this new bifunctional probe can signal whether *none*, *only one*, or *both* receptors are bound by spectroscopically clearly distinguishable outputs and can accordingly communicate e.g. the inputs *none*, *little*, and *much* in the case of a single analyte and different concentration regimes. Its analyte selectivity can be improved by combined measurement of emission spectra and lifetimes. Moreover, this sensor molecule belongs to the very few examples of CT-operated fluorescent probes that reveal a coordination-induced fluorescence enhancement with the classical fluorescence quencher Hg(II).

REFERENCES

1. J. P. Desvergne and A. W. Czarnik (Eds.) (1997). *Chemosensors of Ion and Molecule Recognition*, Kluwer Academic Publishers, Netherlands, and specific reviews referenced in the various chapters.
2. B. Valeur and J.-C. Brochon (Eds.) (2001). *New Trends in Fluorescence Spectroscopy: Applications to Chemical and Life Sciences*, Springer, Berlin, and more specific reviews are referenced in the various chapters.
3. K. Rurack and U. Resch-Genger (2002). Rigidization, preorientation and electronic decoupling—The magic triangle for the design of highly efficient fluorescent sensors and switches. *Chem. Soc. Rev.* **31**, 116, and references therein.
4. K. Rurack (2001). Flipping the light switch 'ON'—The design of sensor molecules that show cation-induced fluorescence enhancement with heavy and transition metal ions. *Spectrochim. Act A* **57**, 2161–2180, and references therein.
5. J. F. Callan, A. P. de Silva, and D. C. Magri (2005). Luminescent sensors and switches in the early 21st century. *Tetrahedron Lett.* **61**, 8551–8588, and references therein.
6. J. F. Callan, A. P. de Silva, and D. C. Magri (2000). Special issue on luminescent sensors. *Coord. Chem. Rev.* **205**, and references therein.

7. S. R. Adam, J. P. Y. Kao, G. Grynkiewicz, A. Minta, and R. Y. Tsien (1988). Biologically useful chelators that release Ca^{2+} upon illumination. *J. Am. Chem. Soc.* **103**, 3212–3220.

8. M. M. Martin, P. Plaza, Y. H. Meyer, F. Badaoui, J. Bourson, J.-P. Lefevre, and B. Valeur (1996). Steady-state and picosecond spectroscopy of Li^+ or Ca^{2+} complexes with a crowned merocyanine. Reversible photorelease of cations. *J. Phys. Chem.* **100**, 6879–6888.

9. P. Plaza, I. Leray, P. Changenet-Barret, M. M. Martin, and B. Valeur (2002). Reversible bulk photorelease of strontium ion from a crown ether-linked merocyanine. *Chem. Phys. Chem.* **3**, 668–674.

10. R. Mathevet, G. Jonusauskas, C. Rullière, J.-F. Létard, and R. J. Lapouyade (1995). Picosecond transient absorption as monitor of the stepwise cation-macrocycle decoordination in the excited singlet state of 4-(*N*-monoaza-15-crown-5)-4′-cyanostilbene. *Phys. Chem.* **99**, 15709–15713.

11. N. Marcotte, P. Plaza, D. Lavabre, S. Fery-Forgues ,and M. M. Martin (2003). Calcium photorelease from a symmetrical donor–acceptor–donor bis-crown-fluoroionophore evidenced by ultrafast absorption spectroscopy. *J. Phys. Chem. A* **107**, 2394–2402.

12. R. Rudolf, M. Mongillo, R. Rizzuto, and T. Pozzan (2003). Innovation: Looking forward to seeing calcium. *Nat. Rev.* **4**, 579–586.

13. Y. Q. Li, J. L. Bricks, U. Resch-Genger,V. Kharlanov and W. Rettig,CT-operated fluorescent reporters with acceptor and donor-receptors: Part I. Photophysical properties and protonation studies of biphenyl-type probes incorporating 2,2′:6′,2″-terpyridine acceptors, *J. Phys. Chem. A.*, manuscript in preparation.

14. Y. Q. Li, J. L. Bricks, U. Resch-Genger, and W. Rettig, CT-operated fluorescent reporters with acceptor and donor-receptors: Part II. Cation coordination behavior of biphenyl-type probes incorporating 2,2′:6′,2″-terpyridine acceptors, *Phys. Chem. Chem. Phys.*, manuscript in preparation.

15. Y. Q. Li, J. L. Bricks, U. Resch-Genger, W. Weigel, and W. Rettig, CT-operated fluorescent reporters with acceptor and donor-receptors: Part III. Spectroscopic, protonation and complexation behavior of biphenyls incorporating 2,2′:6′,2″-bisthienylpyridine binding sites, manuscript in preparation.

16. W. Goodall and J. A. G. Williams (2001). A new highly fluorescent terpyridine which responds to zinc ions with a large red shift. *Chem. Commun.*, 2514–2515.

17. D. Braun, W. Rettig, S. Delmond, J.-F. Letard, and R. Lapouyade (1997). Amide derivatives of DMABN—A new class of dual fluorescent compounds. *J. Phys. Chem.* **101**, 6836–6841.

18. J.-P. Malval and R. Lapouyade (2001). Derivatization of 4-(dimethylamino)benzamide to dual fluorescent ionophores: Divergent spectroscopic effects on N or O amide chelation. *Helv. Chim. Acta* **84**, 2439–2451.

19. K. Hamasaki, H. Ikeda, A. Nakamura, A. Ueno, F. Toda, I. Suzuki, and T. Osa (1993). Fluorescent sensors of molecular recognition. Modified cyclodextrins capable of exhibiting guest-responsive twisted intramolecular charge transfer fluorescence. *J. Am. Chem. Soc.* **115**, 5035–5041.

20. K. Hamasaki, A. Ueno, F. Toda, I. Suzuki, and T. Osa (1994). Molecular recognition indicators of modified cyclodextrins using twisted intramolecular charge-transfer fluorescence. *Bull. Chem. Soc. Jpn.* **67**, 516.

21. W. Siebrand (1966). Mechanism of radiationless triplet decay in aromatic hydrocarbons and the magnitude of the Franck–Condon factors. *J. Chem. Phys.* **44**, 4055–4061.

22. J. Bourson, J. Pouget, and B. Valeur (1993). Ion-responsive fluorescent compounds. 4. Effect of cation binding on the photophysical properties of a coumarin linked to monoaza- and diaza-crown ethers. *J. Phys. Chem. A* **97**, 4552–4557.

23. I. Leray, J.-L. Habib-Jiwan, C. Branger, J.-Ph. Soumillion, and B. Valeur (2000). Ion-responsive fluorescent compounds. VI. Coumarin 153 linked to rigid crowns for improvement of selectivity. *J. Photochem. Photobiol. A* **132**, 163–169.

24. P. Crochet, J.-P. Malval, and R. Lapouyade (2000). New fluoroionophores from aniline dimer derivatives: A variation of cation signalling mechanism with the number of amino groups. *Chem. Commun.*, 289–290.

25. S. Delmond, J.-F. Létard, R. Lapouyade, R. Mathevet, G. Jonusauskas, and C. Rullière (1996). Cation-triggered photoinduced intramolecular charge transfer and fluorescence red-shift in fluorescence probes. *New J. Chem.* **20**, 861–869.

26. S. Fery-Forgues, M. T. Le Bris, J.-P. Guette, and B. Valeur (1988). Ion-responsive fluorescent compounds. 1. Effect of cation binding on photophysical properties of a benzoxazinone derivative linked to monoaza-15-crown-5. *J. Phys. Chem.* **92**, 6233–6237.

27. S. Fery-Forgues, M. T. Le Bris, J.-C. Mialocq, J. Pouget, W. Rettig, and B. Valeur (1992). Photophysical properties of styryl derivatives of aminobenzoxazinones. *J. Phys. Chem.* **96**, 701–710.

28. K. Rurack, W. Rettig, and U. Resch-Genger (2000). Unusually high cation-induced fluorescence enhancement of a structurally simple intrinsic fluoroionophore with a donor–acceptor–donor constitution. *Chem. Commun*, 407–408.

29. N. Marcotte, P. Plaza, D. Lavabre, S. Fery-Forgues, and M. M. Martin (2003). Calcium photorelease from a symmetrical donor–acceptor–donor bis-crown-fluoroionophore evidenced by ultrafast absorption spectroscopy. *J. Phys. Chem. A.* **107**, 2394–2402.

30. B. Liu and H. Tian (2005). A ratiometric fluorescent chemosensor for fluoride ions based on a proton transfer signaling mechanism. *J. Chem. Mater.* **15**, 2681–2686.

31. K. Rurack, A. Koval'chuck, and J. L. Bricks (2001). A simple bifunctional fluoroionophore signaling different metal ions either independently or cooperatively. *J. Am. Chem. Soc.* **123**, 6205–6206.

32. J. N. Wilson and U. H. F. Bunz (2005). Switching of intramolecular charge transfer in cruciforms: Metal ion sensing. *J. Am. Chem. Soc.* **127**, 4124–4125.

33. M. Maus, W. Rettig, and R. Lapouyade (1996). Photodynamics of a pretwisted donor–acceptor biphenyl. *J. Inf. Recording.* **22**, 451–456.

34. W. Rettig, M. Maus, and R. Lapouyade (1996). Conformational control of electron transfer states: Induction of molecular photodiode behaviour. *Ber. Bunsenges. Phys. Chem.* **100**, 2091–2096.

35. M. Maus and W. Rettig (1998). The electronic structure of 4-(*N,N*-dimethylamino)-4′-cyano-biphenyl and its planar and twisted model compounds. *Chem. Phys.* **218**, 151–162.

36. M. Maus and W. Rettig (1998). Donor–acceptor-biphenyls: Electronic and conformational pathways after photoexcitation. *J. Inf. Record.* **24**, 461–468.

37. M. Maus, W. Rettig, G. Jonusauskas, R. Lapouyade, and C. Rulliere (1998). Sub-picosecond transient absorption of donor-acceptor biphenyls. Intramolecular control of the excited state charge transfer processes by a weak electronic coupling. *J. Phys. Chem. A* **102**, 7393–7405.

38. M. Maus, W. Rettig, D. Bonafoux, and R. Lapouyade (1999). Photoinduced intramolecular charge transfer in a series of differently twisted donor–acceptor biphenyls as revealed by fluorescence. *J. Phys. Chem. A* **103**, 3388–3401.

39. M. Maus and W. Rettig (2000). The influence of conformation and energy gaps on optical transition moments in D–A biphenyls. *Chem. Phys.* **261**, 323–337.

40. M. Maus and W. Rettig (2001). Comparison of the bandshape and lifetime data analysis of temperature-dependent fluorescence measurements. A new approach to reveal an excited state conformational equilibrium. *Phys. Chem. Chem. Phys.* **3**, 5430–5437.

41. M. Maus and W. Rettig (2002). The excited state equilibrium between two rotational conformers of a sterically restricted donor–acceptor biphenyl as characterised by global fluorescence decay analysis. *J. Phys. Chem. A* **106**, 2104–2111.

42. Z. R. Grabowski, K. Rotkiewicz, and W. Rettig (2003). Structural changes accompanying intramolecular electron transfer—Focus on T.I.C.T. States and structures. *Chem. Rev.* **103**, 3899–4031.

43. J. P. Malval, J. P. Morand, R. Lapouyade, W. Rettig, G. Jonusauskas, J. Oberlé, C. Trieflinger, and J. Daub (2004). Structural modelling of optical and electrochemical properties of 4-aminodiphenylamines—Optoelectronic studies on a polyaniline repeating unit. *Photochem. Photobiol. Sci.* **3**, 939–945.

44. M. Maus and K. Rurack (2000). Monitoring pH and Solvent proticity with donor–acceptor-substituted biphenyls: A new approach towards highly sensitive and powerful fluorescent probes by tuning the molecular structure. *New J. Chem.* **24**, 677–686.

45. R. M. Izatt, K. Pawlak, J. S.Bradshaw, and R. L. Bruening (1991). Thermodynamic and kinetic data for macrocycle interaction with cations and anions. *Chem. Rev.* **91**, 1721–2085.

46. L. Fabbrizzi and A. Poggi (1995). Sensors and switches from supramolecular chemistry. *Chem. Soc. Rev.* **24**,197–202.

47. Gmelins Handbuch der Anorganischen Chemie (1927). Chor, 8th ed., VCH, Berlin.

48. G. J. Fox, J. D. Hepworth, and G. Hallas (1976). *J. Chem. Soc. Perkin I*, 68.

49. U. Resch-Genger, D. Pfeifer, C. Monte, W. Pilz, A. Hoffmann, M. Spieles, K. Rurack, J. Hollandt, D. Taubert, B. Schönenberger, and P. Nording (2005). Traceability in fluorometry: Part ii. Spectral fluorescence standards. *J. Fluoresc.* **15**, 315–336.

50. J. R. Lakowicz (1999). *Principles of Fluorescence Spectroscopy*, 2nd ed., Kluwer Academic/Plenum Press, New York.

51. D. V. Connor and D. Phillips (1984). *Time-Correlated Single-Photon Counting*, Academic Press, London.

52. W. Weigel, W. Rettig, M. Dekhtyar, C. Modrakowski, M. Beinhoff, and A. D. Schlüter (2003). Dual fluorescence of phenyl and biphenyl substituted Pyrene derivatives. *J. Phys. Chem. A* **107**, 5941–5947.

53. Globals Unlimited, Laboratory of Fluorescence Dynamics at the University of Illinois, (1992).

54. J. N. Demas and K. D. Mielenz (1982). *Optical Radiation Measurements*, Vol. 3, 195 ed., Academic Press, New York.

55. J. Bourson and B. Valeur (1989). Ion-responsive fluorescent compounds. 2. Cation-steered intramolecular charge transfer in a crowned merocyanine. *J. Phys. Chem.* **93**, 3871–3876.

56. N. Miyara and A. Suzuki (1995). Palladium-catalyzed cross-coupling reactions of organoboron compounds. *Chem. Rev.* **95**, 2457–2493.

57. M. Beinhoff, W. Weigel, M. Jurczok, W. Rettig, C. Modrakowski, I. Brüdgam, H. Hartl, and A. D. Schlüter (2001). Synthesis and spectroscopic properties of Arene substituted pyrene derivatives as model compounds for fluorescent polarity probes. *Eur. J. Org. Chem.* 3819–3829.

58. T. Ishiyama, Y. Itoh, T. Kitno, and N. Miyaura (1997). Synthesis of arylboronates via the palladium(0)-catalyzed cross-coupling reaction of tetra(alkoxo)diborons with aryl triflates. *Tetrahedron Lett.* **38**, 3447.

59. A. M. Costero, J. Sanchis, S. Gil, V. Sanz, and J. A. G. Williams (2005). Poly(amine) biphenyl derivatives as fluorescent sensors for anions and cations. *J. Mater. Chem.* **15**, 2848–2853.

60. S. Hashimoto and J. K. Thomas (1984). Effect of environment on decay pathways of the singlet excited state of *N,N,N′,N′*-tetramethylbenzidine. *J. Phys. Chem.* **88**, 4044–4049.

61. J. F. Letard, S. Delmond, R. Lapouyade, D. Braun, W. Rettig, and M. Kreissler (1995). New intrinsic fluoroionophores with dual fluorescence: DMABN-Crown4 and DMABN-Crown5. *Rec. Trav. Chim. Pays-Bas.* **114**, 517–527.

62. F. Bernardi, M. Olivucci, and M. A. Robb (1997). The role of conical intersections and excited state reaction paths in photochemical pericyclic reactions. *J. Photochem. Photobiol. A* **105**, 365–371.

63. J. Michl and V. Bonacic-Koutecký (1990). *Electronic Aspects of Organic Photochemistry*, Wiley, New York.

64. G. Hennrich, H. Sonnenschein, and U. Resch-Genger (1999). Redox switchable fluorescent probe selective for either Hg(II) or Cd(II) and Zn(II). *J. Am. Chem. Soc.* **121**, 5073–5074.

65. K. Rurack, M. Kollmannsberger, U. Resch-Genger, and J. Daub (2000). A selective and sensitive fluoroionophore for Hg^{II}, Ag^{I}, and Cu^{II} with virtually decoupled fluorophore and receptor units. *J. Am. Chem. Soc.* **122**, 968–969.

66. L. Prodi, C. Bargossi, M. Montalti, N. Zaccheroni, N. Su, J. S. Bradshaw, R. M. Izatt, and P. B. Savage (2000). An effective fluorescent chemosensor for mercury ions. *J. Am. Chem. Soc.* **122**, 6769–6770.

67. L. Prodi, F. Bolletta, M. Montalti, and N. Zaccheroni (2000). Luminescent chemosensors for transition metal ions. *Coord. Chem. Rev.* **205**, 59–83.

68. K. Rurack, U. Resch-Genger, and W. Rettig (1998). Global analysis of time-resolved emission—A powerful tool for the analytical discrimination of chemically similar Zn(II) and Cd(II) complexes. *J. Photochem. Photobiol. A* **118**, 143–149.